Etching in Chlorine Discharges Using an Integrated Feature Evolution-Plasma Model

Helen H. Hwang[a], Deepak Bose[b], T. R. Govindan, and M. Meyyappan
NASA Ames Research Center
Moffett Field, CA 94035 USA

Abstract

Etching of semiconductor materials is reliant on plasma properties. Quantities such as ion and neutral fluxes, both in magnitude and in direction, are often determined by reactor geometry (height, radius, position of the coils, etc:). In order to obtain accurate etching profiles, one must also model the plasma as a whole to obtain local fluxes and distributions. We have developed a set of three models that simulates Cl_2 plasmas for etching of silicon, ion and neutral trajectories in the plasma, and feature profile evolution. We have found that the location of the peak in the ion densities in the reactor plays a major role in determining etching uniformity across the wafer. For a stove top coil inductively coupled plasma (ICP), the ion density is peaked at the top of the reactor. This leads to nearly uniform neutral and ion fluxes across the wafer. A side coil configuration causes the ion density to peak near the sidewalls. Ion fluxes are thus greater toward the walls and decrease toward the center. In addition, the ions bombard the wafer at a slight angle. This angle is sufficient to cause slanted profiles, which is highly undesirable.

[a] Electronic mail: hwang@dm1.arc.nasa.gov

[b] Eloret Corporation

I. Introduction

The evolution of etching profiles due to plasma processing conditions is of continuing concern in the semiconductor industry. It is critical to achieve an anisotropic etch to achieve straight walls in trenches, especially as linewidths are decreasing to 0.1 μm. Processing variables, such as gas pressure, rf bias voltage, and coil power, control the plasma properties (species densities, fluxes, electric fields, etc.). Differences in processing conditions, as well as in reactor geometries, have been observed to have dramatic impact on the resulting etch profiles on the substrate.[1,2] Although semi-analytic models can estimate etch rates and species fluxes to the wafer reasonably well,[3] any asymmetry that may arise due to processing or geometry concerns will not be captured. In particular, etch profile variation across the wafer cannot be resolved without calculating the differences in ion and neutral fluxes with respect to radial location.

In order to demonstrate the effects of the plasma on etched features, a feature profile evolution model would have to also consider the plasma properties, such as species fluxes, distributions with respect to impact angle of species landing on the wafer, etc. We have developed a suite of models that couples a plasma simulation to a feature profile evolution model via a third simulation which calculates trajectories of ions and neutral species landing on the wafer. The plasma simulation calculates variables such as electric fields, species densities, and average fluxes, which are then used by the Particle-in-Cell (PIC) simulation. The trajectories of ions and neutrals are advanced, generating velocity and angular distributions at specified locations on the wafer. The feature profile simulation uses the normalized distribution functions to calculate the fluxes and etch rate at any given point on the trench.

II. Description of the Model

1. Semiconductor Equipment Modeling Software (SEMS)

Reactor scale modeling is handled by the Semiconductor Equipment Modeling Software, or SEMS. The SEMS code has been described elsewhere[4] and will briefly be described below. SEMS is 2-D in (r, z) and solves the appropriate fluid equations for all species using a finite difference, implicit Gauss-Seidel line relaxation scheme. Mass balance equations are solved for electrons, ions and neutrals, the energy balance equation for electrons, and Maxwell's equations for power coupling. Also included for the species is a self-consistent effective binary diffusion calculation. Bulk fluxes to the wafer are generated which are later used to normalize distribution functions calculated by the PIC simulation.

2. Particle-in-Cell Neutral and Ion Computation (PICNIC)

Since SEMS is a fluid model, the quantities that are calculated are averages (moments of the Boltzmann distribution function). However, the calculation of etch rates on the wafer depends on the angular information of impacting species in two ways. First, the etch yield is dependent on the ion's impacting angle.[5,6] Second, the view factor, or the allowable range of angles for impacting species inside a feature, determines the fluxes of species to a particular point on the trench. Therefore, both velocity and angular distribution functions for species landing on the wafer are required, but these cannot be generated using SEMS. SEMS can only provide quantities such as average fluxes to the wafer, and not angle-dependent fluxes to the wafer. Hence, we have developed a separate, offline simulation to calculate these necessary distribution functions. The Particle-in-Cell Neutral and Ion Computation (PICNIC) calculates neutral and ion trajectories in the entire plasma reactor using bulk plasma quantities generated by

SEMS (*e.g.*, species densities, electron temperature, electric fields). Although PICNIC is fully 3-D in both velocity and space, particle motion is restricted to 2-D in (r, z) for these simulations. Restricting the motion of the particles ensures axisymmetric flow and therefore consistency with the calculations of SEMS. PICNIC calculates ion and neutral trajectories in the following manner. Particles are generated throughout the reactor according to electron-impact source rate functions from SEMS. Particles are generated with an initial Maxwellian velocity distribution, as there is no gas flow in the PICNIC calculation. Particle motion is tracked, assuming ions are accelerated by electric fields (generated from SEMS) and that both ions and neutrals suffer collisions. These heavy species collisions are handled using a null-collision cross section method with velocity-dependent cross sections (see Hwang and Kushner[7]). Both momentum transfer and species altering collisions (*e.g.*, charge exchange, neutralization reactions) are allowed to occur. Neutrals are allowed to collide at the wall and are reemitted with a probability of $(1 - S_n)$, where S_n is the sticking coefficient. All particles retain their original velocity magnitudes and are reemitted from a cosine angular distribution. Cl is assumed to have a sticking coefficient of 0.1 in both SEMS and PICNIC. Cl_2 has a sticking coefficient of zero, but can be removed from the simulation in the reactor at a loss rate determined by the electron impact source (loss) rate. Ions are assumed to have unity sticking coefficients at the walls and therefore are removed from the simulation once they encounter a wall. Because the sheaths are assumed to be thin in an ICP (much smaller than the mean free path), PICNIC assumes that the sheaths are collisionless and that all ions gain energy due to the sheath potential. SEMS calculates electric fields up to the presheath boundary, but not in the sheath itself. Therefore the ions must gain an additional amount of energy while falling through the sheath. For ions landing on the wafer, this gained energy results in a gain of velocity in the axial direction:[8]

$$\varepsilon_z = T_e \ln\left(\frac{M_i}{2\pi m_e}\right)^{1/2}, \text{ and} \qquad [1]$$

$$|v_z|_{\text{gain}} = \sqrt{\frac{2\varepsilon_z}{M_i}}, \qquad [2]$$

where T_e is the electron temperature, and M_i and m_e are the ion and electron masses, respectively.

The trajectories of ions in the plasma use electric fields generated by SEMS, ignoring the acceleration due to the azimuthal component. Statistics of species are collected at specified points on the wafer. Note that since the reactor is considered to be axisymmetric, all points at the same radial position have the same distribution function. This approach is similar to that of Hoekstra and Kushner,[9] with the following differences. PICNIC calculates one distribution function for each neutral and ion species that bombard the wafer at each specified point based on impacting particle velocity and angle relative to the surface. The velocity used for the distribution function is actually the particle's velocity magnitude, or speed. Each distribution function at a point is thus 2-D in nature and is not the product of two separate distributions ($f(|v|,\theta)$ vs. $f(|v|)\cdot f(\theta)$). When collecting statistics at a particular point on the wafer, the trench alignment is assumed to be in the (r, z) plane. These distribution functions that are calculated are capable of capturing any angular asymmetry that may exist. However, this method does increase the computation time. Collecting statistics for a 2-D resolved distribution function requires on the order of 10,000 particles for 1000 iterations. The other difference in methodology from that of Ref. 9 is that PICNIC does not calculate species densities but relies upon values computed from SEMS.

3. Simulation of Profile Evolution using Level Sets (SPELS)

At a particular radial location on the wafer, the fluxes to the trench can be obtained using the velocity and angular distribution functions from PICNIC. We have developed a feature profile evolution simulation, SPELS, which has been described earlier.[10] Here we will provide a brief summary of the approach we use to calculate trench etching. SPELS uses a level set method to track the evolving surface.[11] Therefore, a "flux" must be calculated at each point in the 2-D (x, y) computational domain around the trench. The directed velocity (of either ion or neutral) has the form $|v|\cos(\theta - \xi)$, where $|v|$ is the magnitude of the total velocity, θ is the impacting angle from the normal, and ξ is the angle of the surface from the normal (see Fig. 1). The impacting angle is defined as

$$\theta = \tan^{-1}\left(\frac{v_r}{v_z}\right). \qquad [3]$$

Then the directed flux from the plasma to a point on the surface is

$$\Gamma_{plasma} = \int_{\theta_1}^{\theta_2}\int_{0}^{v_{max}} |v|\cos(\theta - \psi)\cdot f(|v|,\theta)\cdot|v|\, d|v|\, d\theta\,. \qquad [4]$$

Note that Eq. 4 does not include re-emission fluxes from the trench surface. Both ion and neutral fluxes are calculated according to Eq. 4 for each species. The net ion flux is summed over all ion species (Cl^+ and Cl_2^+), and the neutral flux is calculated from the sum of the fluxes of Cl and Cl_2. Re-emission fluxes for neutrals are accomplished using a line-of-sight calculation along the trench. Ion re-emission fluxes are ignored. Assuming that both molecular and atomic chlorine

passivate the surface of the substrate and the ions etch the silicon chlorides, the etch rate can be obtained. We know that the chlorinated surface coverage at each point is[10]

$$\alpha(x,y) = \frac{S_{n0}\Gamma_n(x,y)}{S_{n0}\Gamma_n(x,y) + Y_{Cl}\Gamma_i(x,y)}, \qquad [5]$$

where S_{n0} is the neutral sticking probability, and Y_{Cl} is the Cl removal yield. Both Cl and Cl_2 are assumed to have the same sticking coefficient. This sticking coefficient refers to Cl and Cl_2 sticking to bare silicon and is different from the sticking coefficients mentioned in Section II.2, which assume sticking on metal walls. As of yet, separate sticking coefficients due to different material boundaries in SEMS and PICNIC have not been incorporated. The etch rate *ER* at each point is then

$$ER = \frac{1}{\rho_{Si}} \cdot Y_{Si}(x,y) \cdot \Gamma_i(x,y) \cdot \alpha(x,y), \qquad [6]$$

where ρ_{Si} is the mass density of Si and Y_{Si} is the Si etch yield. The level set equation is used to advance a higher order variable $G(x, y, t)$, in which the plasma-surface interface occurs at $G(x, y, t_0) = 0$, or the zero level set. On the interface, the etch rate is equal to the opposite of the speed (S) of G. In the remaining (x, y) domain, G is updated by solving the level set equation,

$$\frac{dG}{dt} + S|\nabla G| = 0. \qquad [7]$$

Therefore, the trench movement is indirectly tracked as G is advanced. The simulation continues for a user-specified time.

III. Results and Discussion

For the following cases, the conditions given below are assumed for both SEMS and PICNIC. The reactor is a standard ICP 300 mm etch tool. Two configurations, with either a stove top or side coil, are considered. Both cases use chlorine gas at 10 mTorr, 500 W of ICP power, and gas temperature of 500 K. The electron-impact gas collisions are given in Table 1.[12] The heavy particle reactions that are considered in PICNIC are given in Table 2.

The densities of Cl_2^+ and Cl^+ are shown for the two coil configurations in Figs. 2 and 3. The peak ion densities should occur close to the coils due to the high amount of ionization. For the stove top coil case, both ion densities are peaked near the top of the reactor close to the coils, as shown in Fig. 2. The peak occurs mid-reactor, at a radial location around 12 to 14 cm. Thus, the maximum ion flux to the wafer should occur at approximately this same radial location because the ion velocities will not have a strong radial dependence. The maximum Cl^+ density is about 1.6 times that of the maximum density of Cl_2^+ (6.1×10^{10} cm^{-3} vs. 3.7×10^{10} cm^{-3}). For the side coil case, again the ion densities peak near the coil (see Fig. 3). The peaks of the ion densities occur close to the side walls at a radial location of approximately 20 cm. Again, one would expect maximum ion fluxes to the wafer at large radii, with decreasing ion fluxes at locations closer to the reactor's axis of symmetry. The peak ion densities for Cl^+ and Cl_2^+ are comparable at about 5.6×10^{10} cm^{-3}.

The bulk fluxes to the wafer for neutrals and ions computed by the reactor model SEMS for both stove top and side coil configurations are shown in Fig. 4. The fluxes for Cl and Cl_2 are relatively uniform across the wafer for both configurations, as seen in Fig. 4(a). The dominant neutral is atomic chlorine, as Cl_2 is highly dissociated in the plasma. The ion fluxes, however, vary significantly with radial position (see Fig. 4(b)). For the stove top coil case, the Cl^+ flux decreases at outer radii, because the peak in the Cl^+ density occurs mid-radius and drops off at larger radii. Although the Cl_2^+ flux remains relatively constant over the wafer, its magnitude is approximately one-half that of Cl^+. The total ion flux is still small compared to the total neutral flux (for both coil configurations), which means that etching is accomplished in the "ion starved" regime, where the amount of ion flux dictates the etch rate. Therefore one would expect that the spatial non-uniformity of the ion flux would lead to lower etch rates at larger radii for the stove top coil case. However, the opposite scenario is true for the side coil reactor. In this case, both Cl^+ and Cl_2^+ fluxes increase with increasing radii due to the peak ion densities close to the coils. At 15 cm, the total ion flux to the wafer ($Cl^+ + Cl_2^+$) is higher for the side coil case compared with the fluxes at ~3 cm, due to the high ionization near the outer coils. This in turn will lead to higher etch rates at larger radii.

Typical distribution functions of Cl_2^+ and Cl on the wafer at $R = 7.32630$ cm are shown in Fig. 5 for the side coil case. The distribution functions are calculated from PICNIC and are normalized from Eq. 4 from raw counts of particles as they land at specified locations. The distributions at different radial locations across the wafer do not qualitatively vary in a significant fashion. The velocity and angular distribution functions (VADF) are for the side top coil case, although the VADFs for the stove top coil case are qualitatively the same. The recorded velocity of the species when it hits the wafer is actually the velocity magnitude, with the impacting angled

defined as in Eq. 3. The VADF for Cl_2^+, as shown in Fig. 5(a), is very narrow in angular range. The ions gain energy in the axial direction due to the electric field in the sheath. This increase in axial velocity is usually far greater than the thermal ion speed, which leads to a tight distribution as the sheath is collisionless. The average impacting velocity corresponds to roughly 23 eV. In contrast, the VADF for Cl in Fig. 5(b) covers a broad range of angles and represents an isotropic distribution on the surface, or a cosine dependence on impacting angle. The VADF is broadened by the momentum transfer collisions with Cl and Cl_2.

The neutral distribution on the surface is expected to be isotropic, as the neutrals should be isotropic in the plasma due to the dominance of momentum transfer collisions. In the plasma, the distribution of neutrals with respect to angle is uniform. However, on a surface the distribution is no longer uniform but has a cosine angular dependence. The explanation for this is as follows. Given a point O on a surface in the (r, z) plane, define a semi-circle of radius R around the point (see Fig. 6(a)). Let R represent the distance of one mean free path. Then all particles in the semi-circle that arrive on the surface do so without suffering a collision (and subsequently altering their impacting angle). Thus all particles that are collected within ε of the point at a given angle lie within two triangular areas. These triangles are defined by the point O on the wafer, the locations ε and $-\varepsilon$ from the point, and a point P on the semi-circle. The angles defined by the line between P and the surface are ψ and β, and the angle that the line makes relative to the surface normal is θ (or the impacting angle). The area defined by the triangles is proportional to the fluxes at the point O as a function of angle.

The total area of the triangles is:

$$\tfrac{1}{2}\varepsilon R\sin\psi + \tfrac{1}{2}\varepsilon R\sin\beta = \varepsilon R\cos\tfrac{1}{2}(\psi - \beta). \qquad [8]$$

Further, we know that $\psi + \beta = \pi$ and $\theta = (\pi/2) - \beta$. Substituting, the total area A of both triangles is equal to:

$$A = \varepsilon R \cos\theta \,. \qquad [9]$$

This means that the area will be greatest when $\theta = 0$, or at normal incidence, and the area will vanish when $\theta = \pm\pi$. Therefore since the area is proportional to $\cos\theta$, the distribution of particles landing on the wafer should be a function of $\cos\theta$. This cosine dependence is seen in calculations from PICNIC for Cl, as shown in Fig. 5(b). In PICNIC, since we are currently not considering gas flow effects, the number of Cl_2 particles generated is small and statistics are poor on the wafer. Hence for input into SPELS, we assume that Cl_2 has the same cosine dependence as Cl but is normalized to the bulk fluxes calulated in SEMS.

The velocity dependence of the distribution functions (such as those shown in Fig. 5) can be eliminated by integration. This resulting function is the net flux as a function of impacting angle,

$$g(\theta) = \frac{\int f(v,\theta)\cdot v^2 dv}{\iint f(v,\theta)\cdot v^2 dv \cdot \cos\theta \, d\theta} \,. \qquad [10]$$

The degree to which the distributions $f(v,\theta)$ are skewed can be determined by plotting g as a function of angle. These integrated values of g are shown in Figs. 7 and 8. For the stove top coil configuration in Fig. 7, both Cl_2^+ and Cl^+ ions impact the wafer at nearly head-on incidence at

almost all radii. However, at R = 14.8080 cm, the flux $g(Cl^+)$ shows a distinct shift to the positive angle direction and is not centered at zero incidence. Although the amount of shift is small (~ 2°), the resulting etch profiles are sensitive to the ion distributions and will reflect this skew. The increase in the flux of ions that are directed with $\theta > 0$ indicates that at these larger radii, more ions have a directed velocity from the bulk plasma toward the outer wall. In other words, as the ions strike the wafer, their energy is directed toward the sidewall due to acceleration from the center of the plasma. This is due to the peak ion density being located mid-reactor. In contrast, the shift in angular flux for the side coil case occurs in the $\theta < 0$ direction, as shown in Fig. 8. The skew of g is more pronounced at larger radii. This time, ions are accelerated away from the sidewall and toward the center of the plasma, due to the ion peak densities being located near the sidewalls.

These calculated VADFs are then used to calculate the flux at each point in the trench in SPELS. For the following profiles, we assume a normalizing length of L = 0.5 μm and a hard mask thickness of 0.2 L. The trench opening is equivalent to L. The trench evolution is given for every 0.1 of the total simulation time. All other conditions are equivalent to those given in Ref. 10. The profiles at different radial locations are shown in Figs. 9 and 10. For the stove top coil case, all simulations are run for the same amount of time. This time corresponds to the amount of time it takes to etch a depth of L in open space at R = 14.8080 cm. All trenches are tapered in shape, again indicating that the plasma is in the ion-starved regime. The fluxes of Cl and Cl_2 are high (~10^{17} cm^{-2} s^{-1}) and are relatively constant with radius, as seen in Fig. 4. The flux of Cl_2^+ is also fairly constant over the wafer. However, the flux of Cl^+ decreases with increasing radius, leading to an overall decrease in etch depth versus radial location. The profile at R = 14.8080 cm also has a slight slant to the right. This is consistent with the skew in the ion fluxes in the

positive θ direction. With more ions directed toward the right (or $\theta > 0$), etching should increase toward the right side. The difference in etched depth at the center of the trench at the outer location is approximately 14% less than at 2.81780 cm.

The profiles from the side coil reactor are shown in Fig. 10. For these cases, the simulations were run for the time it takes to etch a depth of L at R = 2.81780 cm. The plasma non-uniformities are reflected in the resulting profiles. Again, the profiles are tapered in shape as were the profiles for the stove top coil case. All of the profiles have a slant toward the left, which is due to the shift of the ion fluxes in the $\theta < 0$ direction. This shift is due to the peak ion densities occurring near the sidewall coils. The ions are not accelerated perpendicularly, but at a slight angle to the left, leading to increased etching at an angle. For the side coil cases, the neutral fluxes at larger radii increase slightly, whereas the ion fluxes increase dramatically as shown in Fig. 4. This increase in the ion flux leads to an overall increase in etch rate with increasing radius, which is the opposite trend for the stove top coil case. The non-uniformity of the etched depth is 25% (R = 2.81780 vs. 14.8080 cm), which is far greater than for the stove top coil configuration.

IV. Concluding Remarks

A set of models, ranging from reactor-level to wafer-scale in domain size, was integrated to simulate etching profile evolution. These models calculate the fluxes of neutrals and ions as a function of velocity and angle impacting the wafer. Our approach includes a continuum based plasma code and a PIC simulation to generate distribution functions. A level set code, SPELS, calculates the resulting profiles based on the fluxes generated from SEMS and PICNIC.

Although such distributions were calculated using these specific simulations, SPELS can use data generated from other models and codes. In the present work, we have used these suite of simulators to study etch profiles in chlorine etching of silicon in inductively coupled plasma reactors. No specific experiments have been modeled as complete sets of experimental conditions along with detailed results are not available in the literature. Nevertheless, we have conducted this study in the spirit of similar, model-only studies of etching, including angular distribution calculations and profile simulations.[3, 9, 13-18]

The most influential aspect on the etch profiles for these reactor geometries is the location of the peak of the ion densities. The location of the peak affects the total (bulk) flux of the ions to the surface versus radial location, and also controls the amount of skew, if any, that the impacting ions have. For the stove top coil configuration, the peak occurs at mid-reactor and causes a shift in the ion distribution function. Although the amount of shift is small, the etch rate is sensitive to the angular distribution and the effect is quite pronounced at larger radii. For the side coil cases, the peak in the ion densities occurs at outer radii, near the coils. The ion fluxes are less uniform across the wafer, and the distributions have a noticeable shift toward negative angles. The etching profiles all are slanted and the variations in the etch depth are greater than for the stove top coil case. Thus, the uniformity of the entire plasma can impact the uniformity of the etched profiles. Such geometric concerns can determine the amount of center-to-edge differences across the substrate and the amount of skew in profiles at the wafer edge.

V. Acknowledgments

HHH and DB's work were performed under NASA contract NAS2-99092 to Eloret.

Table 1. Electron impact reactions used in SEMS. Rates are taken from Ref. 12.

Reaction	Type	Rate (cm^3/s) (T_e in eV)
$e + Cl_2 \rightarrow Cl_2^+ + e + e$	Ionization	$2.12802 \times 10^{-8}\ T_e^{0.771} \exp(-11.7/T_e)$
$e + Cl_2 \rightarrow Cl + Cl + e$	Dissociation	$3.99000 \times 10^{-8}\ T_e^{0.115} \exp(-4.43/T_e)$
$e + Cl_2 \rightarrow Cl_2 + e$	E. Exc. B3p	$1.22999 \times 10^{-7}\ T_e^{1.12} \exp(-4.3/T_e)$
$e + Cl_2 \rightarrow Cl_2 + e$	E. Exc. 21p and 21s	$9.4999 \times 10^{-9}\ T_e^{0.861} \exp(-9.0/T_e)$
$e + Cl_2 \rightarrow Cl_2 + e$	Vibrational	$3.1400 \times 10^{-8}\ T_e^{1.41} \exp(-1.35/T_e)$
$e + Cl \rightarrow Cl + e$	E. Exc. 4s	$1.2700 \times 10^{-8} \exp(-10.97/T_e)$
$e + Cl \rightarrow Cl + e$	E. Exc. 4p	$4.7900 \times 10^{-8} \exp(-10.29/T_e)$
$e + Cl \rightarrow Cl + e$	E. Exc. 3d	$1.9900 \times 10^{-8} \exp(-10.06/T_e)$
$e + Cl \rightarrow Cl + e$	E. Exc. 5p	$9.3200 \times 10^{-9} \exp(-11.06/T_e)$
$e + Cl \rightarrow Cl + e$	E. Exc. 4d	$9.2000 \times 10^{-9} \exp(-11.15/T_e)$
$e + Cl \rightarrow Cl + e$	E. Exc. 5d	$5.2000 \times 10^{-9} \exp(-11.12/T_e)$
$e + Cl \rightarrow Cl^+ + 2e$	Ionization	$2.9600 \times 10^{-8}\ T_e^{0.554} \exp(-13.1/T_e)$
$e + Cl_2 \rightarrow Cl^- + Cl$	Diss. attach.	1.0000×10^{-10}
$e + Cl_2^+ \rightarrow Cl + Cl$		$9.6793 \times 10^{-8}\ T_e^{-0.61} \exp(1.82 \times 10^{-6}/T_e)$
$e + Cl^- \rightarrow Cl + 2e$		$2.9455 \times 10^{-8}\ T_e^{0.68} \exp(-3.8/T_e)$

Table 2. Estimated heavy particle reactions used in PICNIC.

Reaction	k (cm^3/s)	σ_0 (cm^2)
$Cl^- + Cl^+ \rightarrow Cl + Cl$	5.00×10^{-8}	
$Cl^- + Cl_2^+ \rightarrow Cl + Cl_2$	5.00×10^{-8}	
$Cl + Cl + M \rightarrow Cl_2 + M$	6.74×10^{-32} (cm^6/s)	
$Cl^+ + Cl_2 \rightarrow Cl + Cl_2^+$		1.00×10^{-15}
$Cl^+ + Cl \rightarrow Cl + Cl^+$		1.00×10^{-15}
$Cl^- + Cl \rightarrow Cl + Cl^-$		1.00×10^{-15}
$Cl_2^+ + Cl_2 \rightarrow Cl_2 + Cl_2^+$		4.40×10^{-15}

Figure Captions

Fig. 1. The etching geometry is a two dimensional rectangular trench in silicon with a hard mask layer. Ions and neutrals impact the substrate at an angle θ with respect to the vertical. Particles landing with $\theta < 0$ have an angle "to the left", and those with $\theta > 0$ land "to the right." The normal to the interface or level set at each point is denoted by $\hat{n}$, and its angle with respect to the vertical is defined as ξ.

Fig. 2. Ion density contours for Cl_2^+ and Cl^+ in a stove top coil ICP. Peaks for both ion densities occur mid-reactor and close to the coils.

Fig. 3. Ion density contours for Cl_2^+ and Cl^+ in a side coil ICP. Peaks occur near the sidewalls, and both densities are comparable in scale.

Fig. 4. Fluxes from the plasma to the wafer as a function of radial location for stove top and side coil cases. Fluxes are calculated from SEMS. (a) Cl and Cl_2, and (b) Cl_t^+ and Cl_2^+.

Fig. 5. Velocity and angular distribution functions (VADFs) for (a) Cl_2^+ and (b) Cl, at R = 7.32630 cm in a side coil ICP. Ion distributions are tightly centered, whereas the neutral distributions are broad and have a cosine dependence indicating isotropy.

Fig. 6. Calculating angular dependence of an isotropic distribution on the wafer. (a) In a semi-circle of radius R with center O, the particles landing at O within ε are drawn from an area defined by P, ε, and O. These triangles have angles with respect to OP of ψ and β. (b) A close-up view of the triangles. The angle θ is defined by $PO\varepsilon$, with segment OP having length R.

Fig. 7. Integrated ion fluxes as a function of impact angle, stove top coil configuration. Integrating g over θ yields the net flux. Integrated fluxes for (a) Cl_2^+ and and (b) Cl^+. Note the shift toward positive angles for R = 14.8080 cm for Cl^+.

Fig. 8. Integrated ion fluxes as a function of impact angle, side coil configuration. Fluxes shown are for (a) Cl_2^+ and (b) Cl^+. All fluxes have a lean toward negative angles, particularly at the larger values of R.

Fig. 9. Etching profiles for the stove top coil configuration at different radial locations. Locations are at (a) 2.81780 cm, (b) 7.32630 cm, and (c) 14.8080 cm. The slanted profile in (c) reflects the shift in the ion angular fluxes shown in Fig. 7.

Fig. 10. Etching profiles for the side coil configuration at (a) 2.81780 cm, (b) 7.32630 cm, and (c) 14.8080 cm. All three profiles are skewed toward the left, which is due to the shift in the ion angular fluxes toward negative angles.

References

[1] M. A. Vyvoda, H. Lee, M. V. Malyshev, F. P. Klemens, M. Cerullo, V. M. Donnelly, D. B. Graves, A. Kornblit, and J. T. C. Lee, *J. Vac. Sci. Technol. A* **16** 3247 (1998).

[2] J.-H. Lee, G.-Y. Yeom, J.-W. Lee, and J.-Y. Lee, *J. Vac. Sci. Technol. A* **15** 573 (1997).

[3] M. Tuda, K. Nishikawa, and K. Ono, *J. Appl. Phys.* **81** 960 (1997).

[4] D. Bose, T. R. Govindan, and M. Meyyappan, *J. Electrochem. Soc.*, **146** 2705 (1999).

[5] J. P. Chang and H. H. Sawin, *J. Vac. Sci. Technol. A* **15** 610 (1997).

[6] J. A. Levinson, E. S. G. Shaqfeh, M. Balooch, and A. V. Hamza, *J. Vac. Sci. Technol. B* **18** 172 (2000).

[7] H. H. Hwang and M. J. Kushner, *Plasma Sources Sci. Technol.* **3** 190 (1994).

[8] M. A. Lieberman and A. J. Lichtenberg, *Principles of Plasma Discharges and Materials Processing* (Wiley, New York, 1994).

[9] R. J. Hoekstra and M. J. Kushner, *J. Appl. Phys.* **79** 2275 (1996).

[10] H. H. Hwang, T. R. Govindan, and M. Meyyappan, *J. Electrochem. Soc.* **146** 1889 (1999).

[11] J. A. Sethian, *Level Set Methods* (Cambridge University Press, Cambridge, England, 1996).

[12] L. G. Christophorou and J. K. Olthoff, *J. Phys. Chem. Ref. Data*, **28** 131 (1999).

[13] T. J. Cotler, M. S. Barnes, and M. E. Elta, *J. Vac. Sci. Technol. B* **6** 542 (1988).

[14] I. V. Katardjiev, G. Carter, M. J. Nobes, S. Berg, and H.-O. Blom, *J. Vac. Sci. Technol. A* **12** 61 (1994).

[15] S. Hamaguchi and M. Dalvie, *J. Vac. Sci. Technol. A* **12** 2745 (1994).

[16] S. D. Athavale and D. J. Economou, *J. Vac. Sci. Technol. A* **13** 966 (1995).

[17] R. J. Hoekstra, M. J. Grapperhaus, and M. J. Kushner, *J. Vac. Sci. Technol. A* **15** 1913 (1997).

[18] T. Panagopoulos and D. J. Economou, *J. Applied Phys.* **85** 3435 (1999).

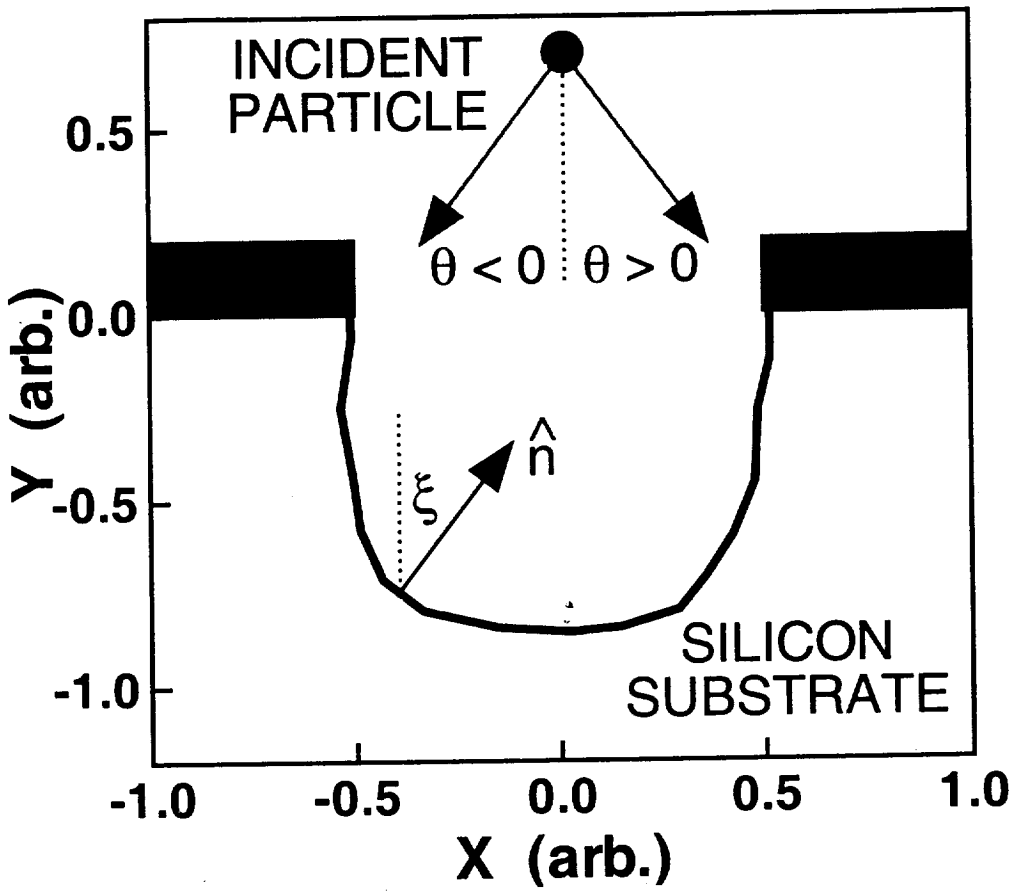
INCIDENT
PARTICLE
θ < 0
θ > 0
n̂
ξ
SILICON
SUBSTRATE
0.5
0.0
-0.5
-1.0
Y (arb.)
-1.0
-0.5
0.0
0.5
1.0
X (arb.)

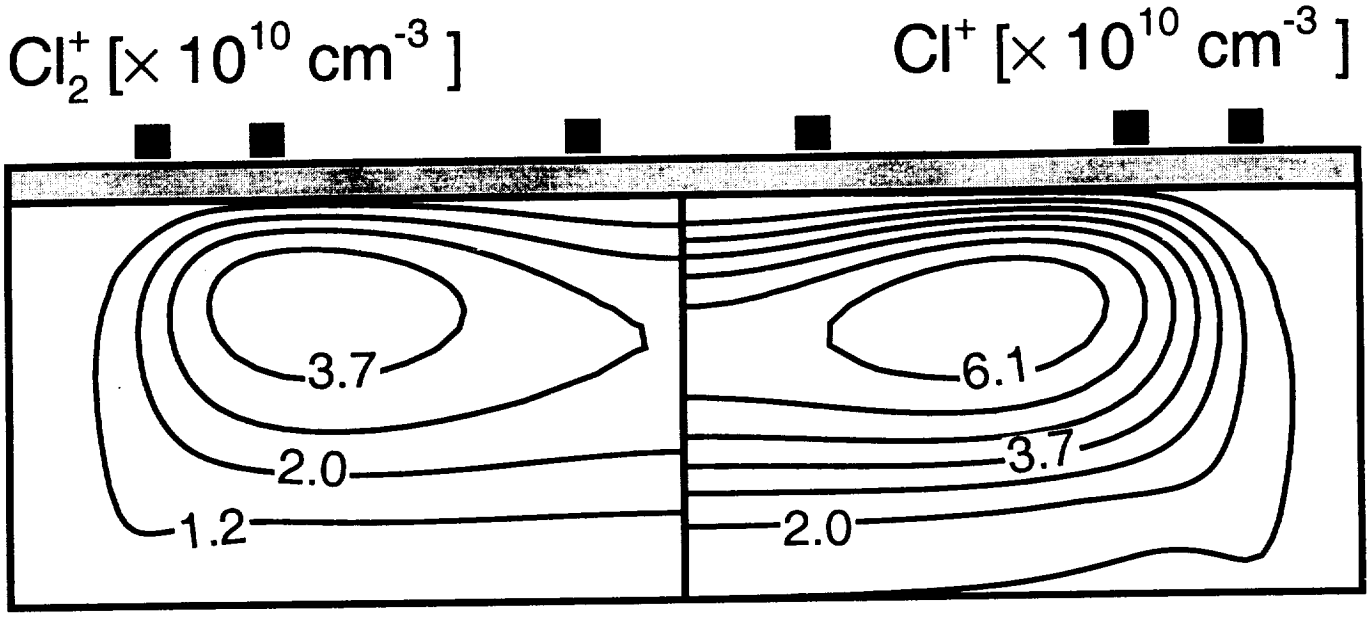
Cl_2^+ [× 10^{10} cm^{-3}]
Cl^+ [× 10^{10} cm^{-3}]
3.7
2.0
1.2
6.1
3.7
2.0

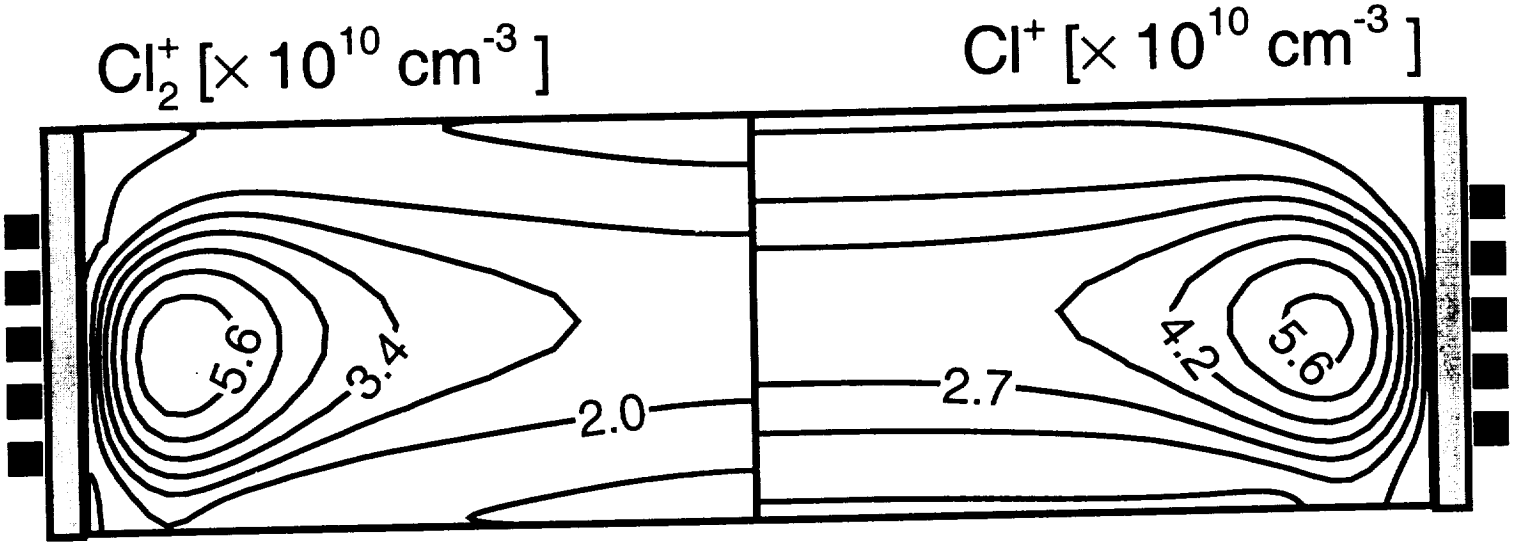
Cl_2^+ [× 10^{10} cm^{-3}]
Cl^+ [× 10^{10} cm^{-3}]
5.6
3.4
2.0
2.7
4.2
5.6

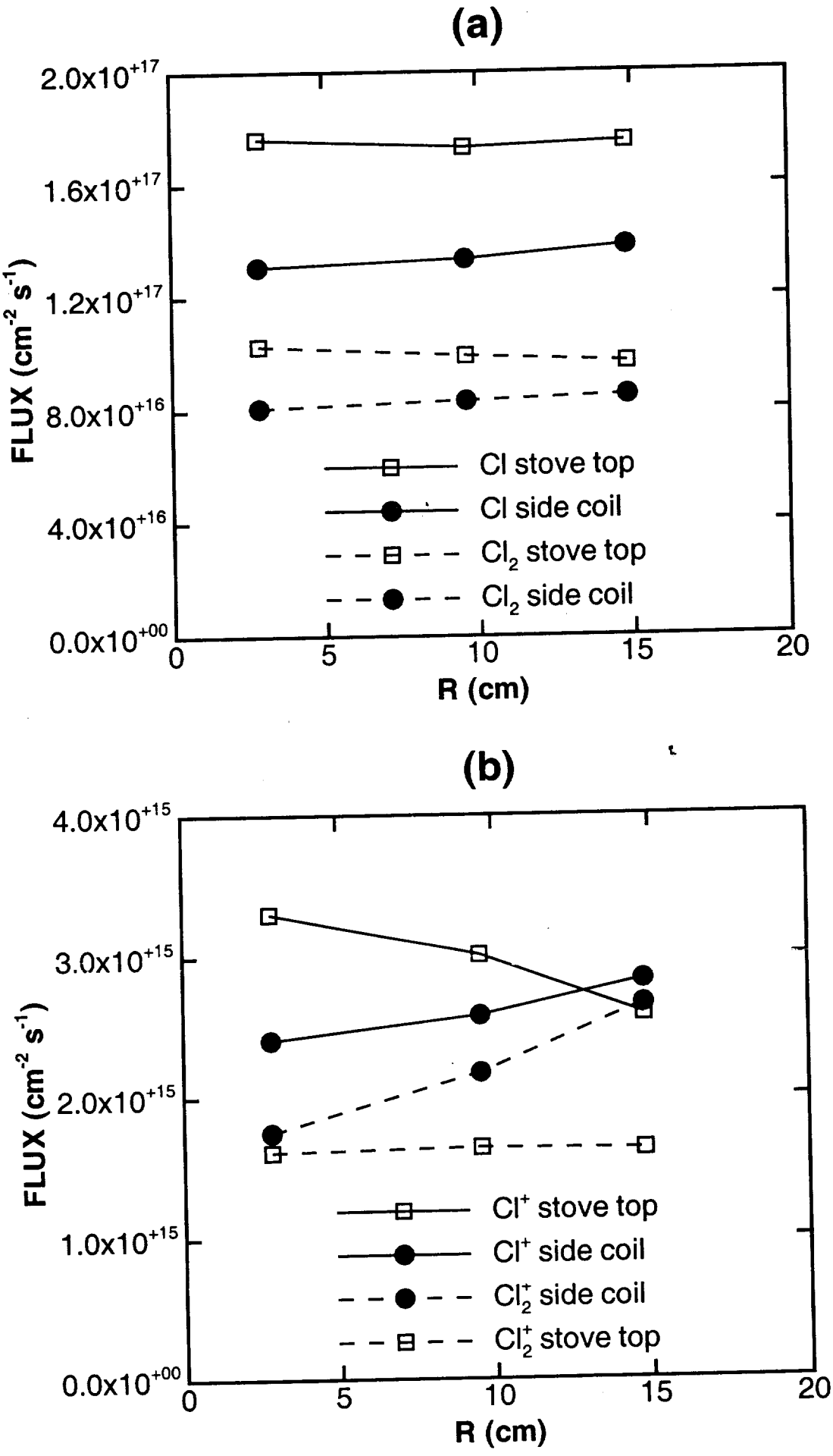

Hwang et al.
Figure 4 of 1

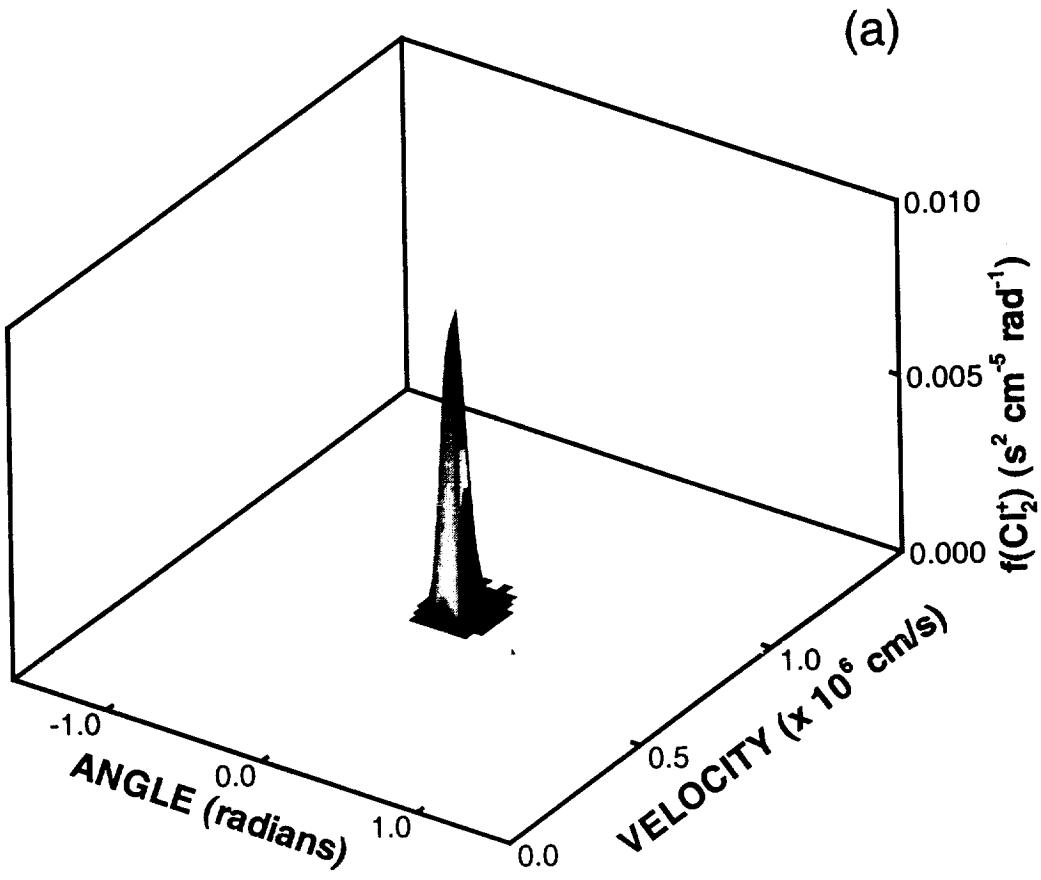

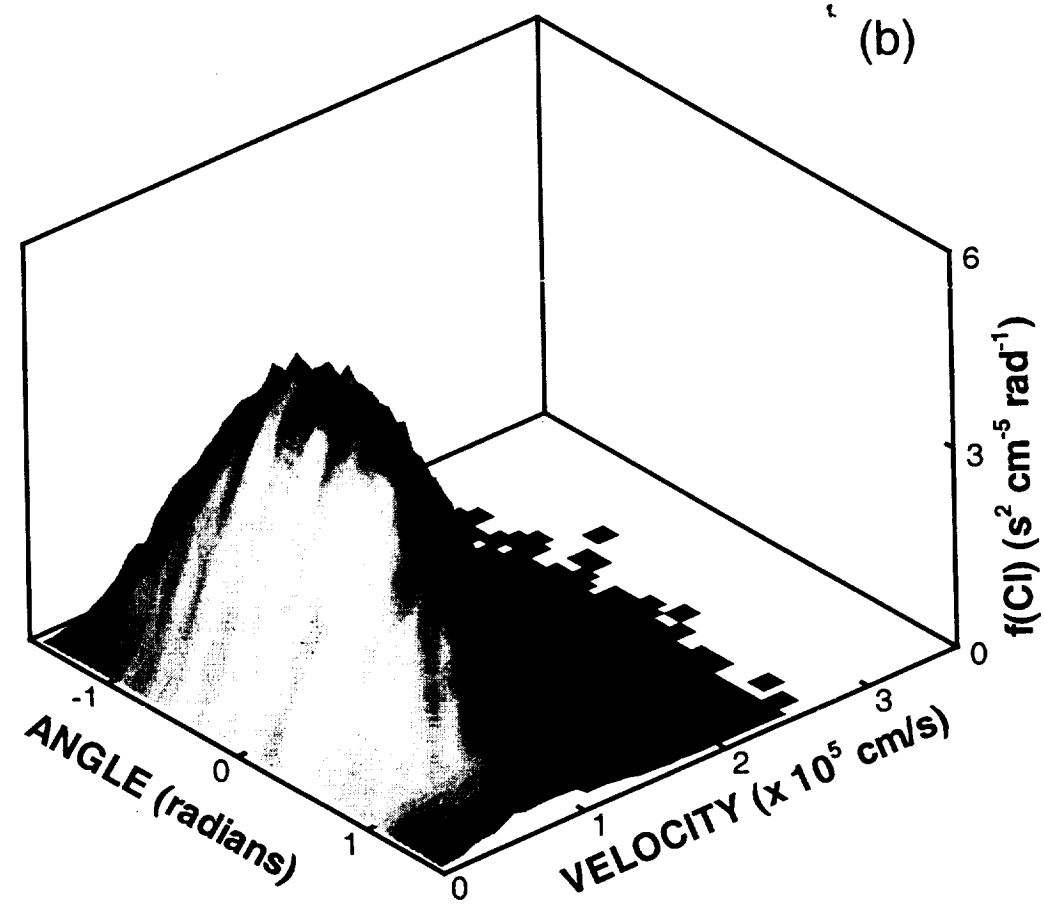

Hwang et al.
Figure 5 of 1

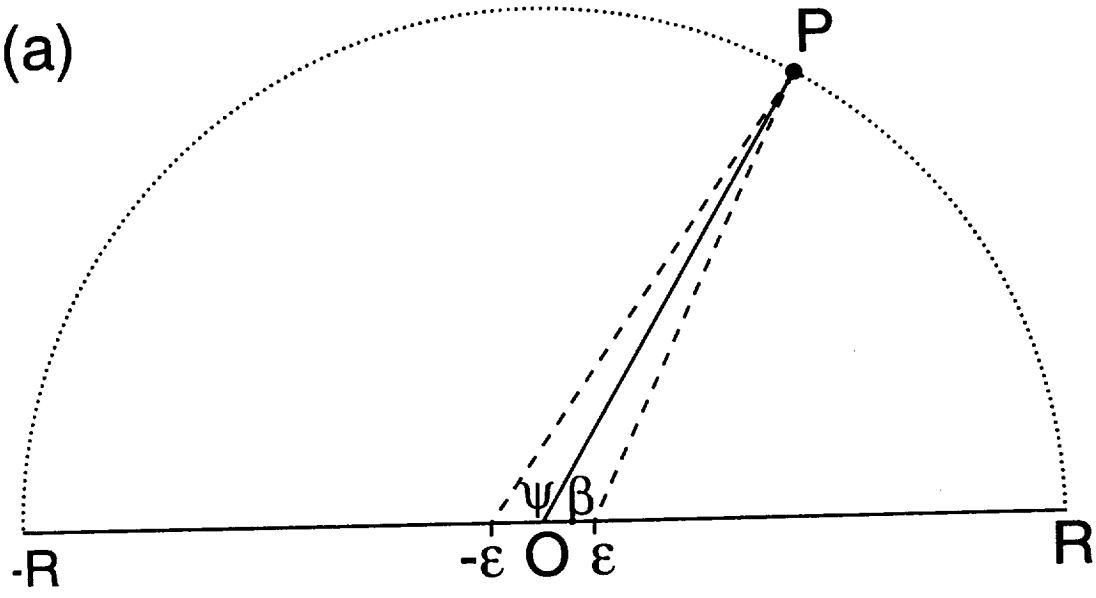

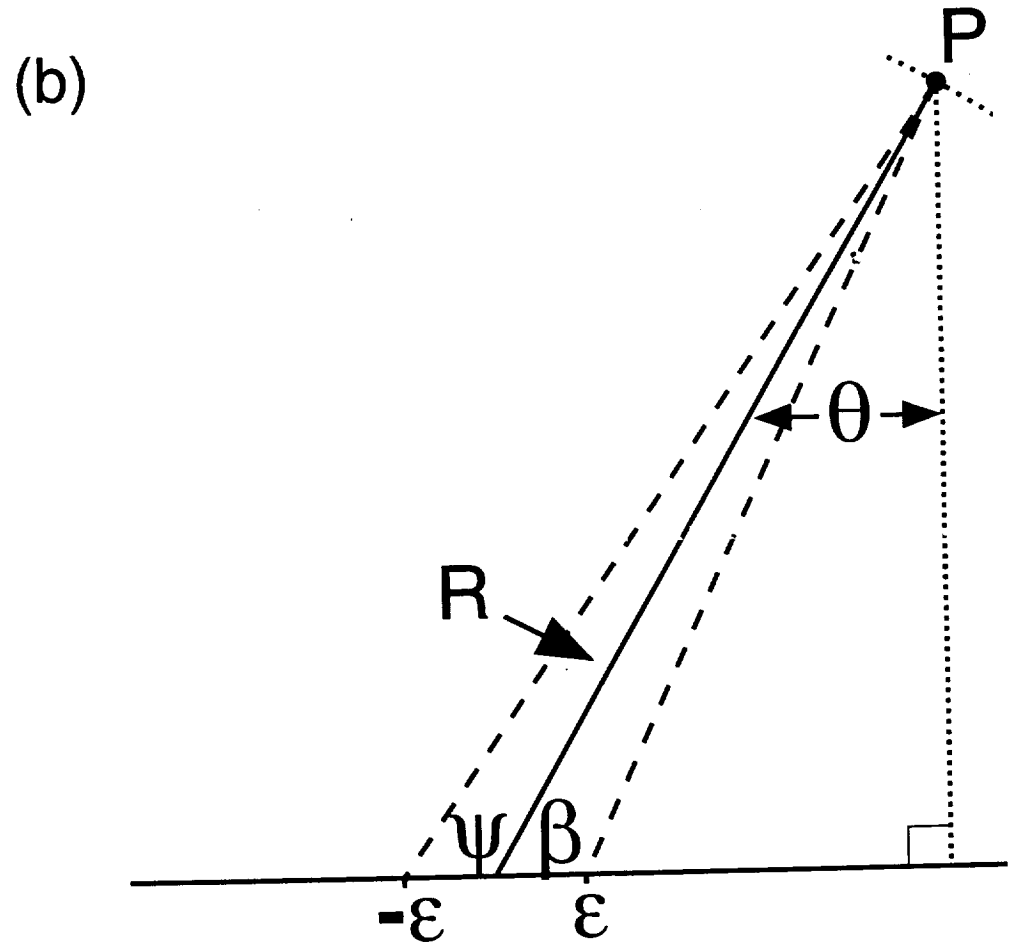

Hwang et al.
Figure 6 of 1

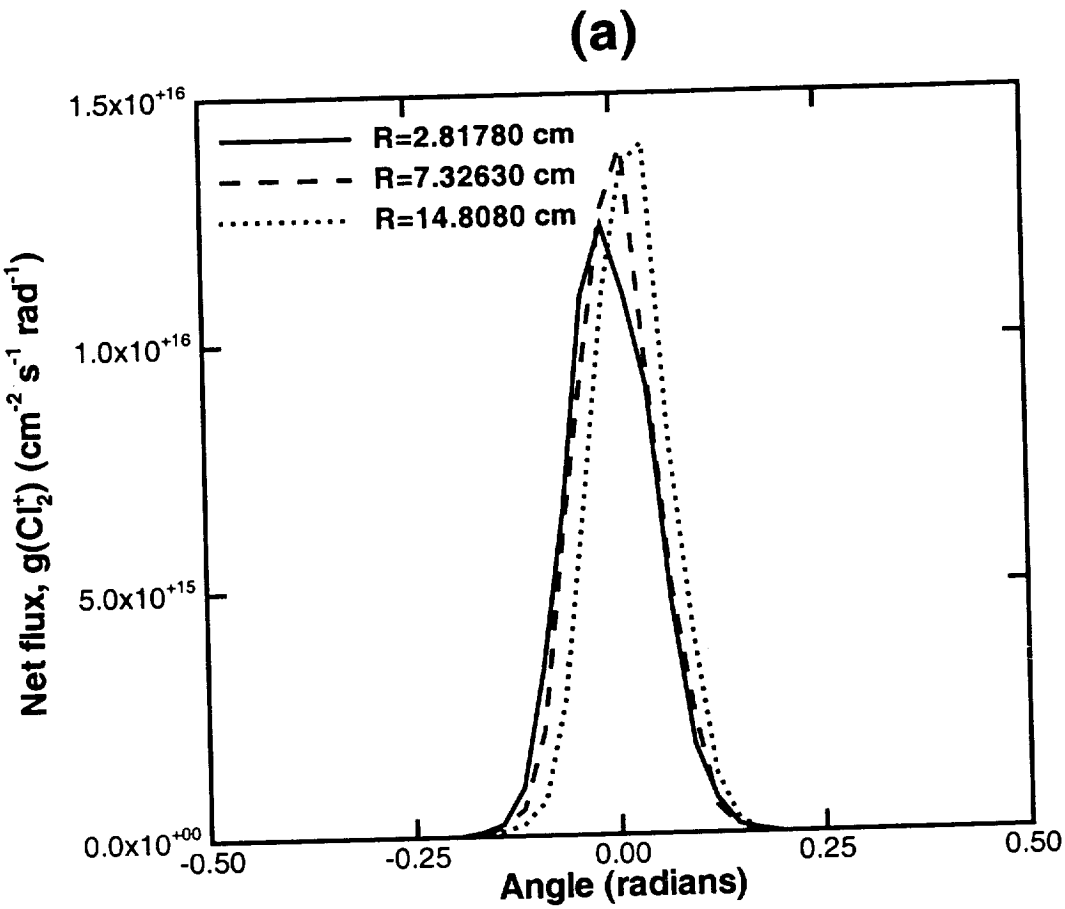

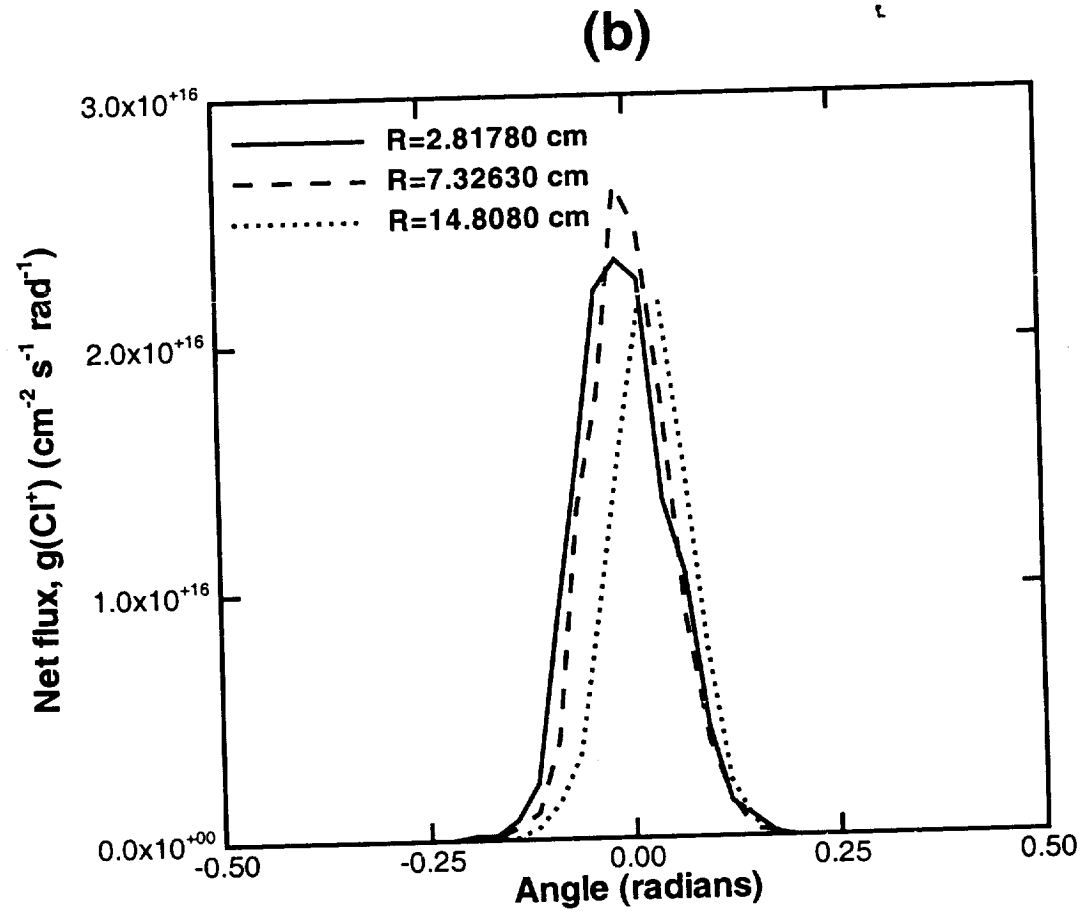

Hwang et al
Figure 7 of

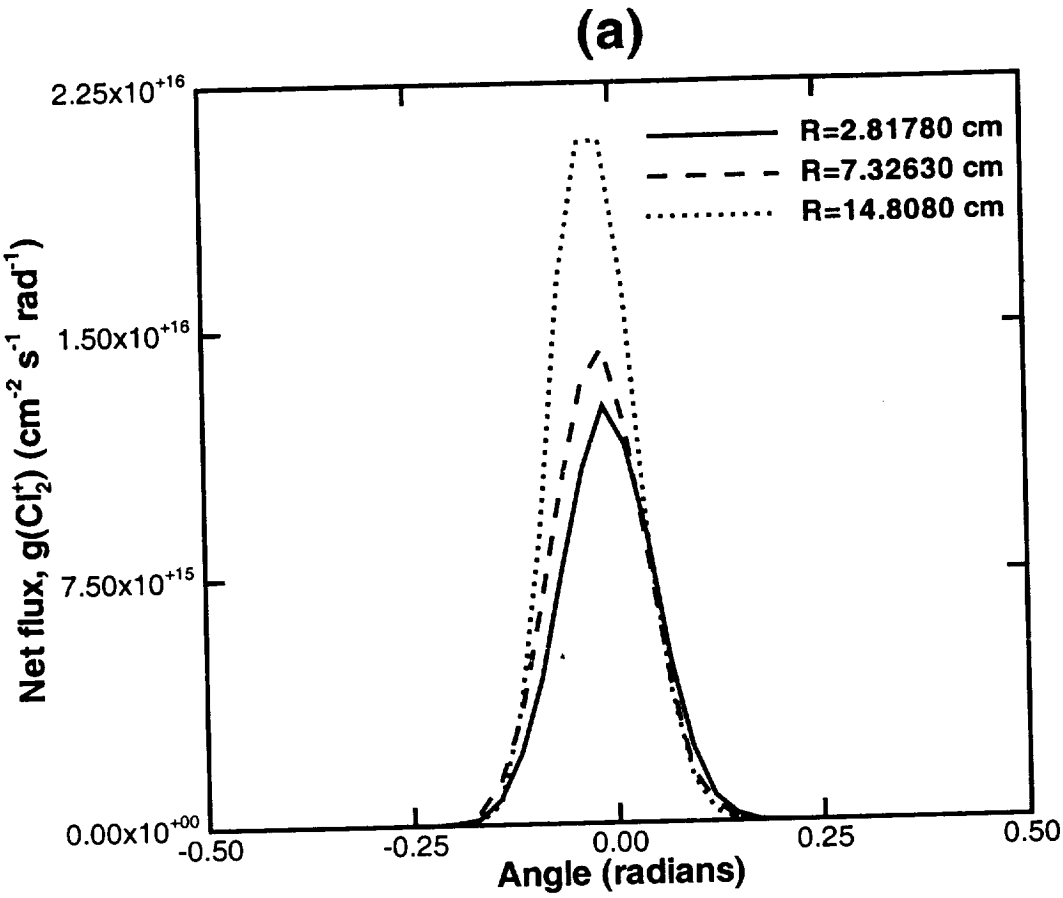

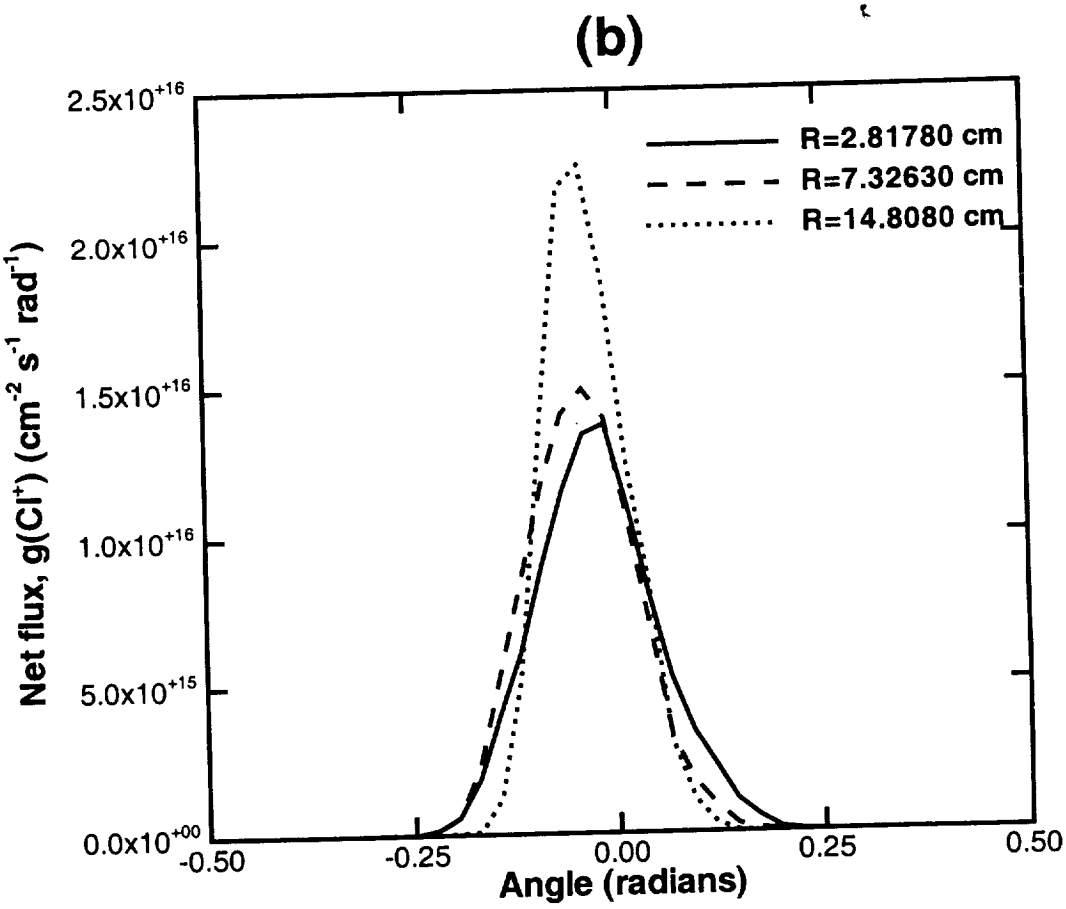

Hwang et al
Figure 8 of

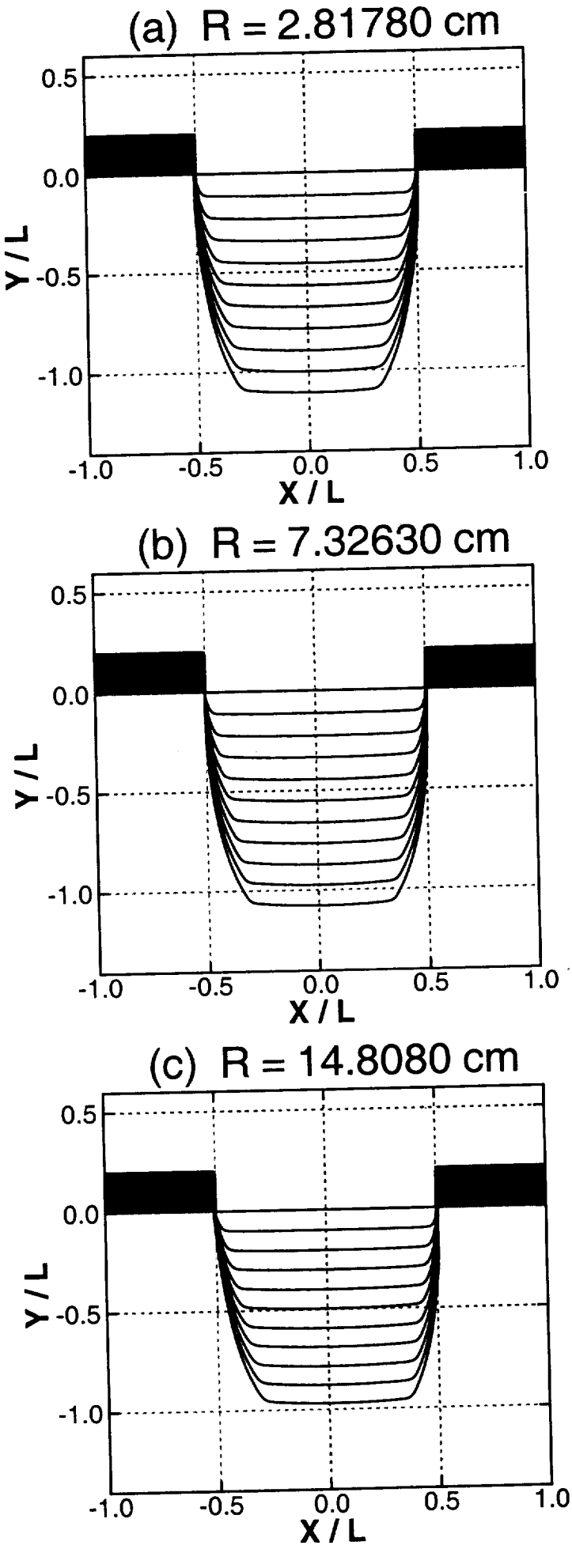
(a) R = 2.81780 cm
0.5
0.0
-0.5
-1.0
Y / L
-1.0
-0.5
0.0
0.5
1.0
X / L
(b) R = 7.32630 cm
0.5
0.0
-0.5
-1.0
Y / L
-1.0
-0.5
0.0
0.5
1.0
X / L
(c) R = 14.8080 cm
0.5
0.0
-0.5
-1.0
Y / L
-1.0
-0.5
0.0
0.5
1.0
X / L

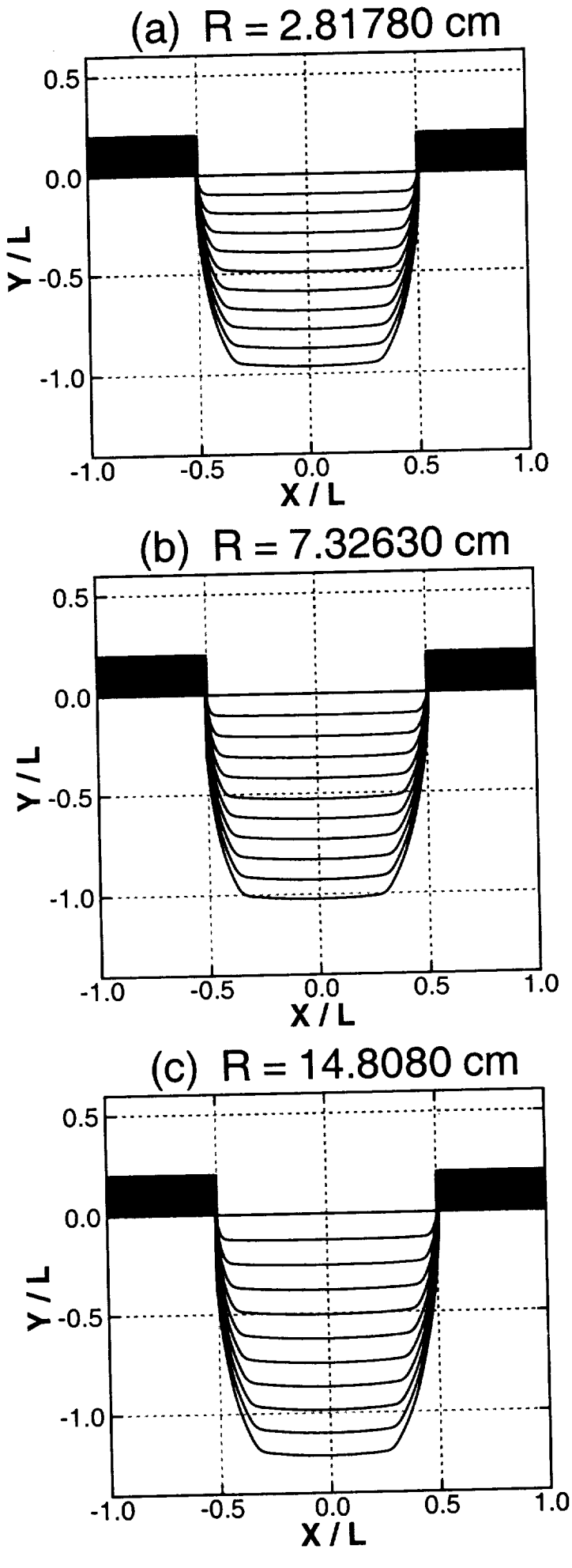

Hwang et a
Fig. 10 of 1